



Newly Identified Hemodynamic Parameter to Predict Thin-Walled Regions of Unruptured Cerebral Aneurysms Using Computational Fluid Dynamics Analysis

Kimura, Hidehito ; Osaki, Susumu ; Hayashi, Kosuke ; Taniguchi, Masaaki ; Fujita, Yuichi ; Seta, Takeshi ; Tomiyama, Akio ; Sasayama, Takashi ...

(Citation)

World Neurosurgery, 152:e377-e386

(Issue Date)

2021-08

(Resource Type)

journal article

(Version)

Accepted Manuscript

(Rights)

© 2021 Elsevier Inc.

This manuscript version is made available under the CC-BY-NC-ND 4.0 license

<http://creativecommons.org/licenses/by-nc-nd/4.0/>

(URL)

<https://hdl.handle.net/20.500.14094/90009137>



A newly identified hemodynamic parameter to predict the thin-walled regions of unruptured cerebral aneurysms using a computational fluid dynamics analysis

Hidehito Kimura, M.D., Ph.D.¹; Susumu Osaki, M.Eng.²; Kosuke Hayashi, D.Eng.²; Masaaki Taniguchi, M.D., Ph.D.³; Yuichi Fujita, M.D., Ph.D.¹; Takeshi Seta, D.Eng.⁴; Akio Tomiyama, D.Eng.²; Takashi Sasayama, M.D., Ph.D.¹; Eiji Kohmura, M.D., Ph.D.^{1,5}

¹Department of Neurosurgery, Kobe University Graduate School of Medicine, Kobe, Japan

²Graduate School of Engineering, Kobe University, Kobe, Japan

³Department of Neurosurgery, Osaka Neurological Institute, Toyonaka, Japan

⁴Graduate School of Science and Engineering for Research, University of Toyama, Toyama, Japan

⁵Department of Neurosurgery, Kinki Central Hospital, Itami, Japan

Corresponding author

Hidehito Kimura, M.D. Ph.D.

Department of Neurosurgery, Kobe University Graduate School of Medicine

7-5-1, Kusunoki-cho, Chuo-ku, Kobe, 650-0017, JAPAN

E-mail: hkimura@med.kobe-u.ac.jp

Key Words: cerebral aneurysm, computational fluid dynamics, OSI, wall thinning, WSS

Short title: OSI can predict thin-walled region

Abstract

Background: The thin-walled regions (TIWR) of intracranial aneurysms has a high risk of rupture during surgical manipulation, which have been reported to be predicted by Wall Shear Stress (WSS) and Pressure (PS) based on Computational Fluid Dynamics (CFD) analysis remain controversial. In this study, we investigated whether the oscillatory shear index (OSI) can predict TIWRs.

Methods: Twenty-five unruptured aneurysms were retrospectively analyzed; the position and orientation of the CFD color maps were adjusted to match the intraoperative micrographs. The red area on the aneurysm wall was defined as TIWR, and if most of the regions on the color map corresponding to TIWR were OSI low (lower quartile range), Time-averaged WSS (TAWSS) high, or PS high (upper quartile range), each region was defined as a matched region, and divided by the total number of TIWRs to calculate the match rate. In addition, the mean values of OSI, TAWSS, and PS corresponding to TIWRs were quantitatively compared with those in adjacent thick-walled regions.

Results: Among 27 TIWRs of 25 aneurysms, 23, 10, 14 regions had low OSI, high TAWSS, and high PS regions (match rate: 85.2%, 37.0%, and 51.9%), respectively. Receiver operating characteristic curve analysis demonstrated that OSI was the most effective hemodynamic parameter (area under the curve, 0.881), followed by TAWSS (0.798). Multivariate analysis showed that OSI was a significant independent predictor of TIWRs (odds ratio, 18.30 [95% CI, 3.2800-102.00], $P < 0.001$).

Conclusions: OSI may be a unique predictor for TIWRs. Low OSI strongly corresponds with TIWRs of IAs.

Introduction

Intracranial aneurysms (IAs) occur in about 2-7% of general population.^{1,2} Most IAs are asymptomatic, but once they rupture, subarachnoid hemorrhage (SAH) occurs, with high mortality and morbidity rates.^{3,4} However, the preventative treatment of IAs, including endovascular surgery or microsurgery, carries a non-negligible risk of morbidity.^{5,6} Therefore, it is essential to identify IAs prone to rupture and to evaluate the balance between the risk and benefit of treatment.^{3,7,8}

The most used determinants for rupture risk are size, location, and growth of the aneurysm.^{4,6} Nevertheless, as many SAHs admitted to the hospital arise from small aneurysms,^{2,9} more reliable characteristics are needed to improve rupture risk assessment.¹⁰

Aneurysm rupture is thought to originate in thin-walled regions (TIWRs).¹¹ Therefore, predicting TIWR may lead to estimation of rupture susceptibility, which may allow for the selection of aneurysms for which surgery is indicated. Furthermore, manipulation of thin-walled regions with surgical instruments may cause intraoperative rupture;¹² this is particularly important in endovascular neurosurgery, in which the aneurysm is not directly visualized.¹³ Therefore, accurate preoperative detection of TIWRs will assist operators in planning their surgical strategy while paying attention to TIWRs to avoid intraoperative rupture.^{12,14,15}

With recent advancements in computational fluid dynamics (CFD) analysis of IAs, two common parameters, namely, wall shear stress (WSS) and pressure (PS), have been reported by several authors as possible parameters for predicting TIWRs.^{10,12,14,16} However, conflicting or inconsistent findings have been noted by different studies, and a consensus has not yet been reached.

We previously reported that the wall shear stress vector cycle variation (WSSVV), which is one of the hemodynamic parameters computed by the commercially available software Hemoscope Ver. 1.5 (EBM Corp., Tokyo, Japan), would be a highly reliable parameter for the detection of TIWRs in IAs.¹⁷ Low WSSVV corresponds to TIWRs. However, WSSVV is a specific parameter to Hemoscope and has not been distributed sufficiently even among CFD researchers. A more familiar CFD parameter in place of WSSVV is necessary.

WSSVV is a parameter that reflects the directional changes in the WSS vector during one cardiac cycle. A high value of WSSVV means large oscillation of the WSS vector on the arterial

wall. Another parameter, oscillatory shear index (OSI), is a common parameter unlike WSSV and is known to reflect fluctuation of the WSS vector along the arterial wall during one cardiac cycle.^{18, 19} In short, both parameters should be consistent in that they reflect WSS vector changes during one cardiac cycle. Hence, we hypothesized that OSI could be a possible parameter to predict TIWRs as well as WSSV. The low OSI regions were hypothesized to correspond with TIWRs.

Originally, IAs have been reported to have a very low OSI uniformly throughout the aneurysm wall.^{16,20,21} The default color bar range of the OSI color map represents values between zero and 0.5, as calculated by the equation. Leemans et al reported that the mean value of OSI in stable and growing aneurysms is 0.01 for both;²⁰ Suzuki et al reported that OSI values are almost zero in the entire domain of the cerebral aneurysms.²¹ Hence, we hypothesized that the color bar range of OSI would to be adjusted toward a lower range to distinguish subtle intra-aneurysmal hemodynamic changes.

In this study, we attempted to adjust the color bar range of the color map of OSI to a smaller range than the default values and investigated whether a low OSI correlates with the TIWRs of UIAs.

Methods

Patient selection

This is a retrospective study. Among 124 consecutive patients underwent aneurysmal neck clipping between April 2013 and August 2019, twenty-five aneurysms in 24 patients met the following inclusion criteria: 1) saccular aneurysm treated by direct surgery, 2) patient age between 20 and 90 years, 3) maximum aneurysm size less than 10 mm, 4) clearly visible aneurysm surface on microscopic observation, and 5) available preoperative high resolution (1.5-tesla) time-of-flight magnetic resonance angiography (TOF-MRA) data. There were 7 men and 17 women (mean age, 61.9 ± 9.79 years; mean aneurysmal neck diameter, 3.2 ± 1.2 mm; mean aneurysmal length, 5.6 ± 1.7 mm; mean aneurysmal width 4.8 ± 2.1 mm) with a total of 18 aneurysms in the middle cerebral artery, 8 in the internal carotid artery and one in the anterior communicating artery (Table 1). Aneurysms that were dissecting, fusiform, or clipped after coil embolization were excluded. Ruptured aneurysms were also excluded because of the poor visibility of the aneurysm wall. In relatively large aneurysms, the dome is generally attached to a

86 branched artery, which hinders the accurate geometrical reconstruction of the aneurysm shape
87 and the arterial branches in the analysis process. Hence, aneurysms whose longest dimension
88 was ≤ 10 mm were also excluded. Furthermore, aneurysms with branches from the dome were
89 excluded because this unusual geometrical condition might skew the results. The aneurysm sizes
90 were measured by two independent engineers.

91 Herein, we report our work according to the “Strengthening the Reporting of
92 Observational Studies in Epidemiology” statement.²² The study was conducted in accordance
93 with the guidelines and under the approval of the local ethics committee of our institution
94 (#180322), and written informed consent was obtained from all patients.

96 **Intraoperative video**

97 Intraoperative video recording was performed in all cases by using a Leica M530 OH6
98 surgical microscope (Leica Microsystems, Wetzlar, Germany) or the Carl Zeiss OPMI
99 PENTERO 900 surgical microscope (Zeiss, Oberkochen, Germany) with a 3-chip CCD (charge-
100 coupled device) color digital video camera at 1920×1080 resolution during aneurysm clipping
101 procedures. Representative intraoperative photographs of the aneurysm dome were extracted
102 from the video data. Special care was taken to evaluate multiple projections of each aneurysm to
103 avoid mischaracterization due to the focal microscope light reflection artifact off of the dome.
104 Regions of the dome were categorized into five grades according to the previous reports that red-
105 walled regions have TIWRs and white- to yellow-walled regions have thick-walled regions
106 (TKWRs): Grade I; red, translucent region with extreme thinning; Grade II, light red, region
107 partially containing whitish coloration; Grade III, whitish pink region, similar to a normal vessel;
108 Grade IV, dark white region; Grade V; yellowish white or yellow arteriosclerotic region. (Figure
109 1)^{7,23}. In this study, Grade I and II regions were classified as TIWRs, and Grade IV and V
110 regions were classified as TKWRs. The findings were assessed by 3 independent neurosurgeons
111 (M.T, Y.F., T.S.).

113 **TOF-MRA condition**

114 Three-dimensional TOF-MRA images were acquired using 1.5 Tesla (T) or 3.0T MRI
115 scanners (Achieva 1.5T Nova Dual, Philips; Achieva 3.0T TX Quasar Dual, Philips; Ingenia
116 3.0T R5.1.7, Philips; Taitan 3T, Toshiba Medical Systems). The imaging parameters for three-

dimensional TOF-MRA with these four scanners were as follows: field of view, 207 mm×230 mm, 184 mm×230 mm, 184 mm×230 mm and 200 mm×192 mm; matrix, 140×400, 243×608, 243×608 and 208×272; and repetition time/echo time, 25 ms/6.91 ms, 25 ms/3.45 ms, 25 ms/3.45 ms and 21 ms/3.4 ms. The slice thickness was 1.1 mm for the first three scanners and 1.0 mm for the Taitan 3T. The parameters for each scanner were manufacturer-installed settings and not customized ones.

CFD analysis

We used our in-house CFD software AN2WER to simulate patient-specific hemodynamics in cerebral arteries, reconstructed from time-of-flight magnetic resonance imaging (TOF-MRA) data using methods we have previously reported.²² In brief, the Reynolds number, Re , and the Womersley number, Wo , were set to typical values for cerebral arteries, i.e., $Re = 200$ and $Wo = 2.5$, where $Re = \rho U_0 D / \eta_P$, $Wo = \rho \omega D^2 / 4 \eta_P$, U_0 is the mean inlet velocity, D is the circle-area-equivalent inlet diameter, ρ is the density, η_P is the reference viscosity, and ω is the angular frequency of pulsatile blood flow. The unsteady flow rate of blood was given as a simple function of time, which was obtained by simplifying a cardiac beat condition¹², to model the typical pulsatile flow. More details for the inlet condition can be found in our previous report²³. The non-Newtonian characteristics of blood were accounted for by means of the Casson model for viscous stress. It should be noted, however, that the Bingham number, Bi , in cerebral arteries is typically small, e.g., 0.1, such that the non-Newtonian effect on blood flow is expected to be small. The Bingham number is defined as $Bi = \tau_0 D / \eta_P U_0$, where τ_0 is the yield stress. The following lattice Boltzmann equation was numerically solved to obtain the velocity and pressure fields, \mathbf{u} and P , as follows:

$$f_i(\mathbf{x} + \mathbf{c}_i \Delta t, t + \Delta t) = f_i(\mathbf{x}, t) + \Omega(f)$$

where f_i is the discrete velocity distribution function of the i th particle group, \mathbf{x} is the Cartesian coordinates, t is the time, Δt is the time step size, \mathbf{c}_i is the particle velocity of the i th particle group. The collision operator $\Omega(f)$ was evaluated using the multiple-relaxation time model. The D3Q19 discrete velocity model was utilized for f_i and \mathbf{c}_i . The no-slip boundary condition at the artery wall was expressed by using the interpolated bounce-back scheme. The density, the velocity and the pressure were obtained by

$$\rho = \sum_{i=0}^{Q-1} f_i$$

$$\rho \mathbf{u} = \sum_{i=0}^{Q-1} \mathbf{c}_i f_i$$

$$P = \rho c_s^2$$

where c_s is the lattice speed of sound and $Q = 19$. The WSS at a point, \mathbf{x}_W , on the artery wall ($\mathbf{u}_W = \mathbf{0}$) was calculated as $\text{WSS} = \eta |\mathbf{u}_t| / \psi$, where η is the non-Newtonian viscosity, \mathbf{u}_s is the tangential component of the velocity at the lattice point closest to \mathbf{x}_W , i.e. $\mathbf{u}_s = (\mathbf{I} - \mathbf{n}\mathbf{n}) \cdot \mathbf{u}$, \mathbf{I} is the unit tensor, \mathbf{n} is the unit normal to the wall, and ψ is the distance between the lattice point and \mathbf{x}_W . The WSS vector, $\boldsymbol{\tau}_t$, was therefore given by $\boldsymbol{\tau}_t = \eta \mathbf{u}_s / \psi$. By averaging $\boldsymbol{\tau}_t$ for the cardiac cycle of a period T , we obtained TAWSS as

$$\text{TAWSS} = \frac{1}{T} \int_0^T |\boldsymbol{\tau}_t| dt$$

The OSI was calculated by

$$\text{OSI} = \frac{1}{2} \left(1 - \frac{\left| \int_0^T \boldsymbol{\tau}_t dt \right|}{\int_0^T |\boldsymbol{\tau}_t| dt} \right)$$

The pressure at the lattice point was used as the pressure, PS, at \mathbf{x}_W . In this study, the viscous shear stress values in the evaluation of TAWSS and OSI were scaled by $\rho U_0^2 / 2$, which is the time-averaged dynamic pressure in a parent artery, to clearly show the magnitude of the shear stresses in cerebral aneurysms compared with the kinetic energy of the blood flow in parent arteries.

Postprocessing

We calculated three hemodynamic indices: (a) the OSI, (b) the time-averaged WSS (TAWSS), and (c) the PS. As described above, to discriminate subtle regional differences more precisely, we attempted to compare four color maps with ranges of zero to 0.5, zero to 0.1, zero to 0.01, and zero to 0.001. In this study, we selected the range of zero to 0.01 as the optimal color bar range to distinguish focal differences on the aneurysm dome (Figure 2).

Match rate of the OSI, WSS, and PS for predicting TIWRs

CFD 3D color maps were manually adjusted to the maximal accordant position of surgical orientation in the video as previous researchers have done.²⁴ TIWRs were marked manually on the intraoperative micrographs and manually transferred to CFD color maps and compared. In this study, we attempt to ensure that low OSI, high TAWSS, high PS correspond to TIWRs. Therefore, on the OSI color map, when the marked TIWRs mostly contained blue or light blue areas indicating the lower quartile range of values across the entire aneurysm surface, the area was determined to have low OSI and counted as a matched region to TIWR. On the other hand, on the TAWSS and PS color maps, when the marked TIWRs mostly contained yellow to red areas, which were equivalent to the upper quartile range of values across the entire aneurysm surface, the areas were determined to have high TAWSS and PS and counted as a matched region to TIWRs. The match rate was calculated as the total number of matched regions to TIWRs divided by the total number of TIWRs marked among all 25 aneurysms.

Quantitative analysis

Not only TIWRs but also TKWRs on each color map were marked and transferred to CFD color maps. Inside the encircled area of each TIWR and TKWR on the color maps of all 25 aneurysms, ten points were selected manually by the two biomedical engineers who were not familiar with the intraoperative photos to ensure no bias was present, and the quantitative values of the three parameters were calculated individually. The mean value of each parameter at the 10 regions was calculated and statistically compared between TIWRs and TKWRs (Figure 3).

Statistical analysis

All continuous quantitative data are shown as the mean \pm SD, and categorical variables are shown as percentages.

For univariate analysis, we used Student's t-test or the Mann-Whitney U test after evaluating the normality of all CFD parameters (OSI, TAWSS, and PS) using the Shapiro-Wilk normality test. Post-hoc power analysis was performed to evaluate whether our data had sufficient verification power; the power criterion for validation was defined as > 0.8 . The receiver operating characteristic curve was used to identify the optimal threshold separating TIWRs and TKWRs by calculating the area under the receiver operating characteristic curve (AUC). Spearman's rank correlation test was performed to examine the potential correlations

between OSI, WSS and PS. The degree of association was interpreted as follows: strong (absolute value of correlation coefficient, $|r| = 0.7-1$), moderate ($|r| = 0.5-0.7$), or low ($|r| = 0.3-0.5$).

For multivariate analysis, logistic regression analysis was performed to clarify independent hemodynamic factors related to TIWRs after excluding parameters with multiple collinearity.

All statistical analyses were performed with EZR (Saitama Medical Center, Jichi Medical University, Saitama, Japan), which is a graphical user interface for R 3.4.3 (R Foundation for Statistical Computing, Vienna, Austria). A two-sided $P < 0.05$ was considered statistically significant.

Results

Match rate of PS, WSS, and OSI for predicting TIWRs (Figure 4)

Out of the 25 aneurysms, seven aneurysms did not have TIWR. Among the remaining 18 aneurysms, 27 regions with Grade I or II regions were marked as TIWRs. Among those 27 regions, 23 had low OSI, 10 had high TAWSS, and 14 had high PS (match rate: 85.2%, 37.0%, 51.9%, respectively).

Quantitative analysis of TIWRs and TKWRs

Out of the 25 aneurysms, four aneurysms did not have TKWR. Among the remaining 21 aneurysms, twenty-two regions with Grade IV or V regions were classified as TKWRs. Hence, 27 TIWRs and 22 TKWRs were investigated. The differences in the OSI and TAWSS values were statistically significant ($P < 0.0001$ and $P < 0.001$, respectively), while not significant for PS ($P = 0.433$) (Figure 5). According to the power analysis, the OSI and TAWSS analyses had sufficient power (0.975 and 0.888, respectively); however, those for PS did not have sufficient power (0.236). There was a moderate correlation between OSI and TAWSS ($|r| = 0.589$, $P = .000021$), while no apparent correlation was found between OSI and PS ($|r| = 0.0892$, $P = 0.56$) or between TAWSS and PS ($|r| = 0.212$, $P = 0.163$) (Figure 6). Receiver operating characteristic curve analysis demonstrated that OSI was the most effective hemodynamic parameter for detecting TIWRs in cerebral aneurysms (AUC, 0.881; 95% confidence interval, 0.768–0.995; cutoff value, 0.006; sensitivity, 0.870; specificity, 0.864) (Figure 7), followed by TAWSS (AUC, 0.798; 95% confidence interval, 0.670–0.927; cutoff value, 0.032; sensitivity, 0.826; specificity,

0.882) (Table 2). Multivariate analysis showed that OSI was a significant independent predictor of TIWRs (odds ratio, 18.300 [95% CI, 3.280-102.000], $P < 0.001$) (Table 3).

Discussion

To the best of our knowledge, this is the first report which clarified that OSI is a reliable parameter to predict TIWRs of UIAs. Regions with low OSI on the color map strongly correlated with TIWRs on the aneurysm dome. High TAWSS tended to correlate to TIWRs, however, high PS did not correspond to TIWRs in this study.

OSI and WSS

The OSI has been reported to be a possible marker for atherosclerosis.^{19,25,26} Regions with high OSI values in the aorta and carotid bifurcation have atherosclerosis.^{19,25,27} Furukawa et al reported that high OSI might be the most valuable hemodynamic parameter to detect TKWRs of cerebral aneurysms.²⁵ Given these results that high OSI correlates with wall thickness and atherosclerosis, it can be postulated that conversely, low OSI correlates with wall thinning. However, no author has successfully demonstrated such a finding.

As previously reported, the default color map of OSI itself tends to demonstrate few regional differences and homogenously very low values over the UIAs.^{20,21} Only after we had appropriately adjusted the color bar range of the OSI color map, set from zero to 0.01 in this study, we successfully distinguished between TIWRs and TKWRs on the color map. This is the reason why researchers have not detected the variation.¹⁴ Furukawa et al showed unintentionally in their paper that TIWRs of UIAs had low OSI values and relatively high WSS values, which appeared to be statistically significant; however, this pattern was not discussed because the authors focused on the TKWRs of the UIAs rather than the TIWRs.²⁵

The OSI is a parameter reflecting WSS vector changes during one cardiac cycle. A low OSI indicates regions where the WSS vector hardly changes, pointing only unidirectionally, which causes a high WSS.²⁸ On the other hand, a high OSI indicates regions where the WSS vector changes multidirectionally on the arterial walls during one cardiac cycle, indicating the occurrence of blood stagnation and low WSS.²⁹⁻³⁰ As we successfully demonstrated in this study, WSS and OSI values tended to correlate inversely for the abovementioned reason. Low OSI possibly correlates with High WSS.

WSS acts as a force tangential to the local vessel walls. High WSS can activate mural cells and act as a dysplastic force against the vessel walls, which is a reported mechanism for the creation of TIWRs.³¹ Other authors reported that focally high WSS is associated with endothelial cell depletion and might cause aneurysm wall thinning, possibly leading to aneurysm rupture.^{21, 32,33} These reports support our finding that low OSI and high TAWSS correlate with TIWRs.

However, there have been several conflicting reports regarding WSS. Some authors demonstrated that low WSS correlates with TIWRs of cerebral aneurysms.^{10,14, 34} The precise reasons for the conflicting results remain unresolved. There may be not only methodological differences but also complex interactions among aneurysm geometry, hemodynamics and wall remodeling.¹⁴ Since we failed to show a statistically significant difference in our multivariate analysis, WSS would likely not provide definitive findings in predicting TIWRs.

Pressure

Recently, pressure has been reported to be a reliable parameter for detection of TIWRs.^{12,14,35} Jiang et al speculated that this mechanism is the direct stress of hemodynamic pressure.¹⁴ In this study, PS did not have sufficient power (power = 0.236), possibly due to the small numbers for PS, which may be the reason that our study failed to show a significant difference. However, quantitative values of TIWRs and TKWRs mostly overlapped in our study (Figure 6). Based on CFD analysis, Kulesár et al reported that the pressure of the color map is relatively uniform, similar to our results.³⁶ As another report does not demonstrate significant difference of pressure in predicting TIWRs, utilizing PS may cause errors in predicting TIWRs.³⁷

Other parameters

We previously reported that WSSVV is able to predict the aneurysm wall condition. Low WSSVV strongly corresponds to TIWRs.¹⁷ WSSVV represents the degree of oscillation on the WSS vector in one cardiac cycle and may be a similar parameter to OSI.¹⁷ By using another parameter, WSS divergence (WSSD), Kim et al demonstrated that high WSSD corresponded to the TIWRs of UIAs.²⁴ WSSD is a hemodynamic parameter that accounts for the net flux of the WSS vector. High WSSD means a net WSS flux diverging away from a point on the wall, whereas low WSSD shows the opposite phenomenon that net WSS flux converges, which can represent flow separation and stagnation, respectively.²⁴ In this regard, WSSD may belong to the

same family as OSI among several CFD parameters, as both reflect WSS vector change and blood stagnation.²⁴ These findings support our results that the regions with unidirectional, not stagnated, blood flow display low OSI on the color map and may cause TIWRs.

Limitations

There are several limitations to our current study. First, this is a retrospective study and the number of cases is relatively small. Second, the identification of TIWRs in intraoperative images is subjective and significantly dependent on the visual judgment of the clinicians. Third, we used TOF-MRA images for the CFD analysis to calculate OSI using our original software.²² We notice that TOF-MRA has lower resolution than the images from computed tomography angiography and rotational angiography. Currently, patients who undergo aneurysm clipping do not receive routine rotational angiography. The computed tomography angiography sometimes depicted the venous system on the same image, which hinders the geometrical reconstruction of the cerebral arteries and causes failure of the CFD analysis. TOF-MRA is a less invasive method to depict the cerebral arteries and usually does not include the venous system on the image. Our original software was designed to solve TOF-MRA and had already been validated.²² Hence, we used TOF-MRA to accomplish the current study. The effects of the low quality of images on the results will be discussed in our future work. Fourth, the OSI color map shows that not only TIWRs but also the parent arteries tend to have homogeneously blue areas. This means that the blood flow in the parent artery is generally unidirectional. Actually, the healthy parent arteries do not suffer from TIWRs because of the possible reason that the parent arteries have normal vessel wall structure. In order to cause thinning of the vessel wall, not only low OSI but also abnormalities in the specific wall structure of the aneurysm wall will be essential. This should be certified by the future histopathological study integrated with the CFD analysis. Sixth, the boundary conditions for the artery wall and the pulsatile inflow in CFD analysis were not patient-specific. The application of patient-specific boundary conditions for CFD analysis would be more desirable. Blood vessels were assumed to be rigid, nonslip walls for simplicity. The elasticity of blood vessel walls should be included in the analysis to clarify the actual pathophysiological phenomenon, which can be implemented by the fluid-structure interaction technique. Introduction of fluid-structure interaction simulation is awaited in future work.

Conclusion

We demonstrated that OSI could predict the TIWRs of UIAs with high accuracy once its color bar range was appropriately adjusted to range from zero to 0.01. Although the optimal color bar range remains uncertain, clinicians could potentially predict the TIWRs of the IAs preoperatively with the familiar CFD parameter OSI. This finding will be beneficial for surgeons in reducing the risk of intraoperative aneurysm rupture not only during open microsurgery but also during endovascular treatment. The latter treatment in particular does not provide direct visualization of the dome intraoperatively. Hence, the current results are expected to be more useful for indicating to endovascular surgeons when they must take caution with certain regions. In deploying the coils around the TIWRs inside the aneurysms, special attention must be devoted to avoiding penetration of the aneurysm wall by the coils. Furthermore, this finding hopefully provides predictive data for future rupture risk and aid in clinical decision making with regard to selecting aneurysms which should be treated after further analysis accumulated.

Acknowledgments

We thank Mr. Noriyuki Negi for assisting with the radiological data analysis. This work was supported by JSPS KAKENHI Grant Number JP 17K10826.

References

1. Vlak MHM, Algra A, Brandenburg R, Rinkel GJE. Prevalence of unruptured intracranial aneurysms, with emphasis on sex, age, comorbidity, country, and time period: A systematic review and meta-analysis. *Lancet Neurol.* 2011;10(7):626-636. doi:10.1016/S1474-4422(11)70109-0
2. Li M-H, Chen S-W, Li Y-D, et al. Prevalence of Unruptured Cerebral Aneurysms in Chinese Adults Aged 35 to 75 Years. *Ann Intern Med.* 2013;159(8):514. doi:10.7326/0003-4819-159-8-201310150-00004
3. Spetzler RF, McDougall CG, Albuquerque FC, et al. The barrow ruptured aneurysm trial: 3-year results: Clinical article. *J Neurosurg.* 2013;119(1):146-157. doi:10.3171/2013.3.JNS12683
4. The Natural Course of Unruptured Cerebral Aneurysms in a Japanese Cohort. *N Engl J Med.* 2012;366(26):2474-2482. doi:10.1056/nejmoa1113260
5. Kotowski M, Naggara O, Darsaut TE, et al. Safety and occlusion rates of surgical treatment of unruptured intracranial aneurysms: A systematic review and meta-analysis of the literature from 1990 to 2011. *J Neurol Neurosurg Psychiatry.* 2013;84(1):42-48. doi:10.1136/jnnp-2011-302068
6. Naggara ON, White PM, Guilbert F, Roy D, Weill A, Raymond J. Endovascular treatment of intracranial unruptured aneurysms: Systematic review and meta-analysis of the literature on safety and efficacy. *Radiology.* 2010;256(3):887-897. doi:10.1148/radiol.10091982
7. Juvela S, Poussa K, Lehto H, Porras M. Natural history of unruptured intracranial aneurysms: A long-term follow-up study. *Stroke.* 2013;44(9):2414-2421. doi:10.1161/STROKEAHA.113.001838
8. Wiebers DO. Unruptured intracranial aneurysms: Natural history, clinical outcome, and risks of surgical and endovascular treatment. *Lancet.* 2003;362(9378):103-110. doi:10.1016/S0140-6736(03)13860-3
9. Weir B, Disney L, Karrison T. Sizes of ruptured and unruptured aneurysms in relation to their sites and the ages of patients. *J Neurosurg.* 2002;96(1):64-70. doi:10.3171/jns.2002.96.1.0064
10. Kadasi LM, Dent WC, Malek AM. Colocalization of thin-walled dome regions with low

- hemodynamic wall shear stress in unruptured cerebral aneurysms. *J Neurosurg.* 2013;119(1):172-179. doi:10.3171/2013.2.JNS12968
11. Kataoka K, Taneda M, Asai T, Kinoshita A, Ito M, Kuroda R. *Structural Fragility and Inflammatory Response of Ruptured Cerebral Aneurysms A Comparative Study Between Ruptured and Unruptured Cerebral Aneurysms.*; 1999. <http://ahajournals.org>. Accessed January 7, 2021.
12. Suzuki T, Takao H, Suzuki T, et al. Determining the Presence of Thin-Walled Regions at High-Pressure Areas in Unruptured Cerebral Aneurysms by Using Computational Fluid Dynamics. *Neurosurgery.* 2016;79(4):589-595. doi:10.1227/NEU.0000000000001232
13. Kadasi LM, Dent WC, Malek AM. Cerebral aneurysm wall thickness analysis using intraoperative microscopy: effect of size and gender on thin translucent regions. *J Neurointerv Surg.* 2013;5(3):201-206. doi:10.1136/neurintsurg-2012-010285
14. Jiang P, Liu Q, Wu J, et al. Hemodynamic characteristics associated with thinner regions of intracranial aneurysm wall. *J Clin Neurosci.* 2019. doi:10.1016/j.jocn.2019.06.024
15. Chen X-L, Chen Y, Ma L, et al. Translucent Appearance of Middle Cerebral Artery Bifurcation Aneurysms Is Risk Factor for Intraoperative Aneurysm Rupture During Clipping. *World Neurosurg.* 2017;101:149-154. doi:10.1016/J.WNEU.2017.01.097
16. Cho K-C, Choi JH, Oh JH, Kim YB. Prediction of Thin-Walled Areas of Unruptured Cerebral Aneurysms through Comparison of Normalized Hemodynamic Parameters and Intraoperative Images. *Biomed Res Int.* 2018;2018:3047181. doi:10.1155/2018/3047181
17. Kimura H, Taniguchi M, Hayashi K, et al. Clear Detection of Thin-Walled Regions in Unruptured Cerebral Aneurysms by Using Computational Fluid Dynamics. 2018. doi:10.1016/j.wneu.2018.09.098
18. Tanaka K, Ishida F, Kawamura K, et al. Hemodynamic Assessment of Cerebral Aneurysms Using Computational Fluid Dynamics (CFD) Involving the Establishment of Non-Newtonian Fluid Properties. *J Neuroendovascular Ther.* 2018;12(8):376-385. doi:10.5797/jnet.oa.2017-0088
19. Ku DN, Giddens DP, Zarins CK, Glagov S. Pulsatile flow and atherosclerosis in the human carotid bifurcation. Positive correlation between plaque location and low and oscillating shear stress. *Arteriosclerosis.* 1985;5(3):293-302. doi:10.1161/01.atv.5.3.293
20. Leemans EL, Cornelissen BMW, Slump CH, Majoie CBLM, Cebral JR, Marquering HA.

Comparing Morphology and Hemodynamics of Stable-versus-Growing and Grown
Intracranial Aneurysms. doi:10.3174/ajnr.A6307

21. Suzuki D, Funamoto K, Sugiyama S, Nakayama T, Hayase T, Tominaga T. Investigation of characteristic hemodynamic parameters indicating thinning and thickening sites of cerebral aneurysms. *J Biomech Sci Eng*. 2015;10(1). doi:10.1299/jbse.14-00265
22. Susumu Osaki, Kosuke Hayashi, Hidehito Kimura, Takeshi Seta, Eiji Kohmura AT. Numerical simulations of flows in cerebral aneurysms using the lattice Boltzmann method with single- and multiple-relaxation time collision models. *Comput Math with Appl*. 2019;78:2746-2760.
23. Kimura H, Hayashi K, Taniguchi M, et al. Detection of Hemodynamic Characteristics Before Growth in Growing Cerebral Aneurysms by Analyzing Time-of-Flight Magnetic Resonance Angiography Images Alone - Preliminary results -. *World Neurosurg*. November 2018. doi:10.1016/j.wneu.2018.11.081
24. Hun Kim J, Han H, Moon Y-J, et al. Hemodynamic Features of Microsurgically Identified, Thin-Walled Regions of Unruptured Middle Cerebral Artery Aneurysms Characterized Using Computational Fluid Dynamics. doi:10.1093/neuros/nyz311
25. Taylor CA, Hughes TJR, Zarins CK. Finite element modeling of three-dimensional pulsatile flow in the abdominal aorta: Relevance to atherosclerosis. *Ann Biomed Eng*. 1998;26(6):975-987. doi:10.1114/1.140
26. Soulis J V., Fytanidis DK, Lampri OP, Giannoglou GD. Low Density Lipoprotein and Non-Newtonian Oscillating Flow Biomechanical Parameters for Normal Human Aorta. *Cardiol Res*. 2016;7(2):66-79. doi:10.14740/CR.V7I2.467
27. Markl M, Brendecke SM, Simon J, Barker AJ, Weiller C, Harloff A. Co-registration of the distribution of wall shear stress and 140 complex plaques of the aorta. *Magn Reson Imaging*. 2013;31(7):1156-1162. doi:10.1016/j.mri.2013.05.001
28. Buchanan JR, Kleinstreuer C, Truskey GA, Lei M. Relation between non-uniform hemodynamics and sites of altered permeability and lesion growth at the rabbit aorto-celiac junction. *Atherosclerosis*. 1999;143(1):27-40. doi:10.1016/S0021-9150(98)00264-0
29. Peiffer V, Sherwin SJ, Weinberg PD. Does low and oscillatory wall shear stress correlate spatially with early atherosclerosis? A systematic review. *Cardiovasc Res*. 2013;99(2):242-250. doi:10.1093/cvr/cvt044

30. Sugiyama S-I, Endo H, Niizuma K, et al. Computational Hemodynamic Analysis for the Diagnosis of Atherosclerotic Changes in Intracranial Aneurysms: A Proof-of-Concept Study Using 3 Cases Harboring Atherosclerotic and Nonatherosclerotic Aneurysms Simultaneously. doi:10.1155/2016/2386031
31. Meng H, Tutino VM, Xiang J, Siddiqui A. High WSS or Low WSS? Complex interactions of hemodynamics with intracranial aneurysm initiation, growth, and rupture: Toward a unifying hypothesis. *Am J Neuroradiol*. 2014;35(7):1254-1262. doi:10.3174/ajnr.A3558
32. Blankena R, Kleinloog R, Verweij BH, et al. Thinner regions of intracranial aneurysm wall correlate with regions of higher wall shear stress: A 7T MRI study. *Am J Neuroradiol*. 2016;37(7):1310-1317. doi:10.3174/ajnr.A4734
33. Cebal JR, Castro MA, Burgess JE, Pergolizzi RS, Sheridan MJ, Putman CM. Characterization of cerebral aneurysms for assessing risk of rupture by using patient-specific computational hemodynamics models. *AJNR Am J Neuroradiol*. 26(10):2550-2559. <http://www.ncbi.nlm.nih.gov/pubmed/16286400>. Accessed December 12, 2019.
34. Kawaguchi T, Nishimura S, Kanamori M, et al. Distinctive flow pattern of wall shear stress and oscillatory shear index: Similarity and dissimilarity in ruptured and unruptured cerebral aneurysm blebs. *J Neurosurg*. 2012;117(4):774-780. doi:10.3171/2012.7.JNS111991
35. Suzuki T, Stapleton CJ, Koch MJ, et al. Decreased wall shear stress at high-pressure areas predicts the rupture point in ruptured intracranial aneurysms. *J Neurosurg*. March 2019:1-7. doi:10.3171/2018.12.JNS182897
36. Kulcsár Z, Ugron Á, Marosfoi M, Berentei Z, Paál G, Szikora I. Hemodynamics of cerebral aneurysm initiation: The role of wall shear stress and spatial wall shear stress gradient. *Am J Neuroradiol*. 2011;32(3):587-594. doi:10.3174/ajnr.A2339
37. Cho K-C, Choi JH, Oh JH, Kim YB. Prediction of Thin-Walled Areas of Unruptured Cerebral Aneurysms through Comparison of Normalized Hemodynamic Parameters and Intraoperative Images. *Biomed Res Int*. 2018;2018:1-9. doi:10.1155/2018/3047181

Figure legends

Figure 1. Categorization of the aneurysm dome into five grades according to the extent of the wall thinning: Grade I; red, translucent region with extreme thinning; Grade II, light red, region partially containing whitish coloration; Grade III, whitish pink region, similar to a normal vessel; Grade IV, dark white region; Grade V; yellowish white or yellow arteriosclerotic region. The regions with Grade I or II lesions were classified as TIWRs, and the regions with Grade IV and V lesions were classified as TKWRs.

(TIWR, thin-walled region; TKWR, thick-walled region)

Figure 2. OSI color map with four different color bar ranges. From left to right, the color bar range has been adjusted to range from 0 to 0.5 (default OSI color map), 0 to 0.1, 0 to 0.01, or 0 to 0.001 in order.

(OSI, oscillatory shear index)

Figure 3. Representative case showing the method of quantitative evaluation for the regions corresponding to the TIWRs and the TKWRs on each color map. A, TIWRs and TKWRs in the intraoperative photographs of the aneurysm dome are encircled by yellow and black circles, respectively; B, 3D-reconstructed models from time-of-flight magnetic resonance angiography showing 10 manually selected points inside each circle, from which the values were calculated. C-E, right upper columns showing each value of the selected 10 points of the TIWRs and right lower columns showing those of the TKWRs in the color maps of OSI (C), TAWSS (D), PS (E), respectively.

(3D, 3-dimensional; OSI, oscillatory shear index; PS, pressure; TAWSS, time-averaged wall shear stress; TIWR, thin-walled region; TKWR, thick-walled region)

Figure 4.

Intraoperative photographs and each CFD color map of all eighteen aneurysms that had TIWRs in order. In the leftmost column, intraoperative photographs are shown. 26 TIWRs are outlined with yellow circles. The next second column presents 3D-reconstructed models from time-of-flight magnetic resonance angiography. The adjacent third, fourth and rightmost columns provide color maps of OSI, TAWSS, and PS, respectively, with the corresponding areas to the

TIWRs encircled by yellow as well. Red asterisks indicate regions with correspondence to TIWRs, where the marked regions had low OSI, high TAWSS, or high PS (23, 10, 14 regions, respectively).

(3D, 3-dimensional; CFD, computational fluid dynamics; OSI, oscillatory shear index; PS, pressure; TAWSS, time-averaged wall shear stress; TIWR, thin-walled region)

Figure 5.

Quantitative evaluation between TIWRs and TKWRs in OSI (A), TAWSS (B), PS (C).

Among 27 TIWRs and 22 TKWRs, the mean values of the selected TIWR vs. TKWR areas on the OSI, TAWSS, and PS color maps were 0.003 ± 0.006 vs. 0.034 ± 0.032 , 0.081 ± 0.068 vs. 0.029 ± 0.019 , and 1685.5 ± 13.8 vs. 1694.3 ± 31.6 , respectively (mean \pm SD). The differences in the OSI and TAWSS values were statistically significant ($P < 0.0001$ and $P < 0.001$, respectively), while it was not significant in PS ($P = 0.433$).

(*: significance at $P < 0.001$, **: significance at $P < 0.0001$, n.s: not significant after Mann-Whitney U test)

(OSI, oscillatory shear index; PS, pressure; TAWSS, time-averaged wall shear stress; TIWR, thin-walled region)

Figure 6.

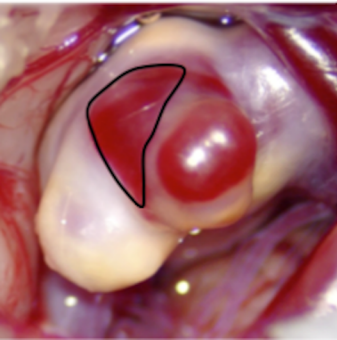
Scatter plot showing Spearman's rank correlation between OSI and TAWSS (left), OSI and PS (middle), and TAWSS and PS (right). A significant (two-tailed) Spearman negative correlation was demonstrated between OSI and TAWSS (moderate; $r = 0.589$, $P < 0.0001$). There was no apparent correlation between OSI and PS or TAWSS and PS ($r = 0.0892$ and 0.212 , respectively; $P = 0.56$ and 0.163 ; respectively).

(OSI, oscillatory shear index; PS, pressure; TAWSS, time-averaged wall shear stress)

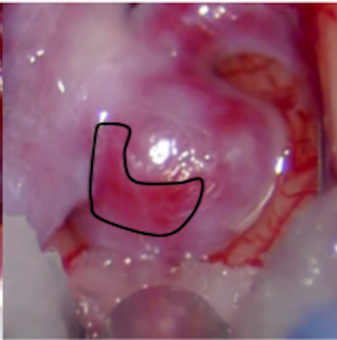
Figure 7. Receiver operating characteristic curve for OSI (AUC, 0.881; 95% confidence interval, 0.768–0.995; cutoff value, 0.006; sensitivity, 0.870; specificity, 0.864)

(AUC: area under the curve; OSI: oscillatory shear index)

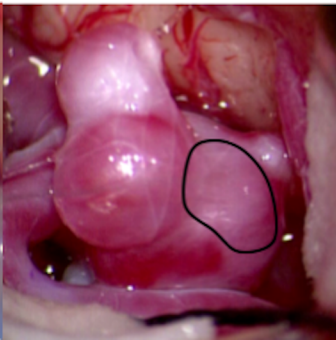
Grade I



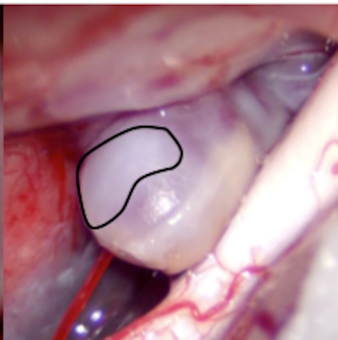
Grade II



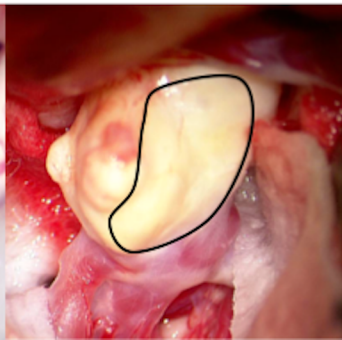
Grade III

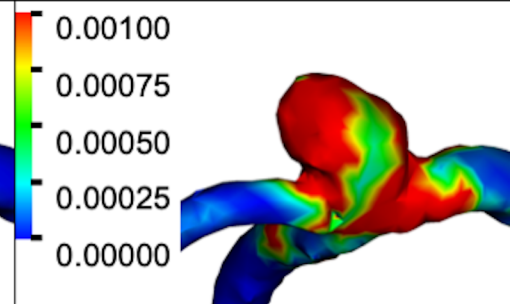
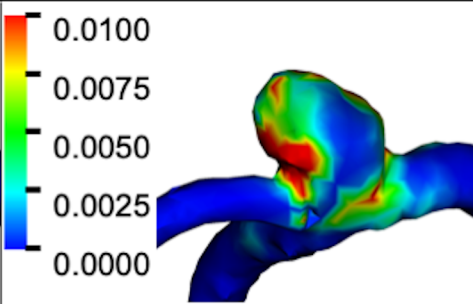
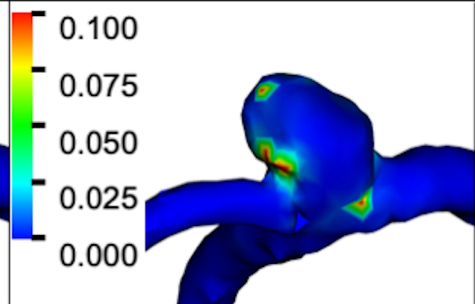
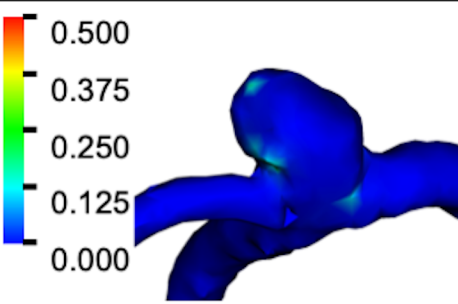


Grade IV

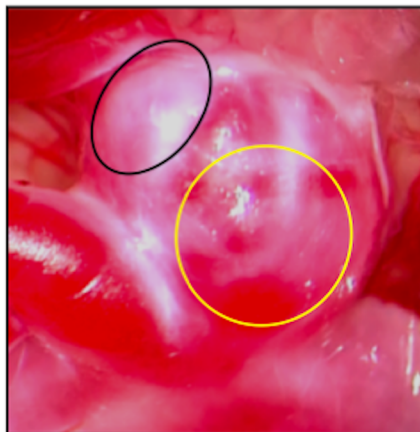


Grade V

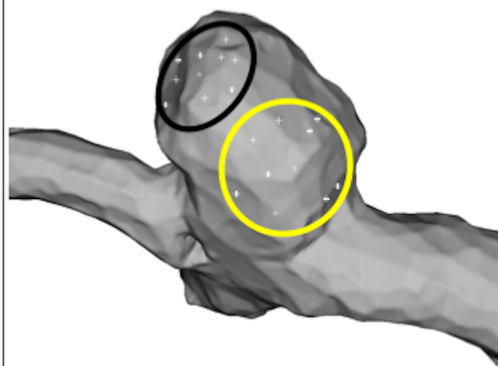




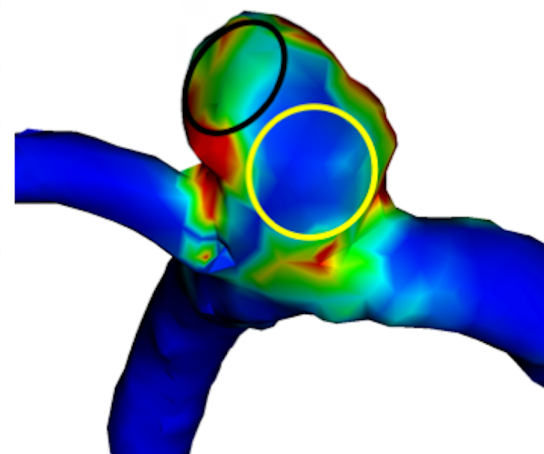
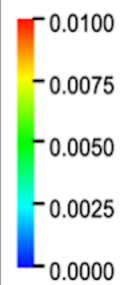
A



B



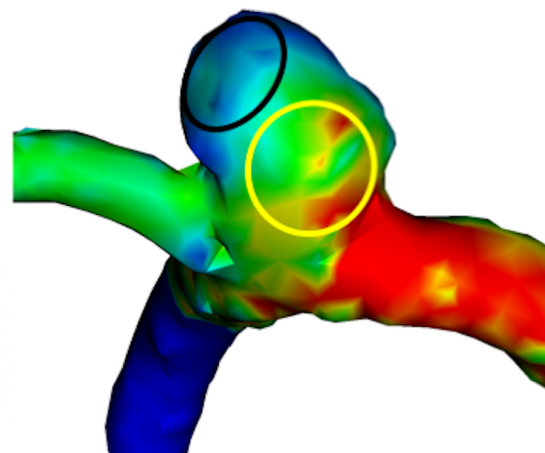
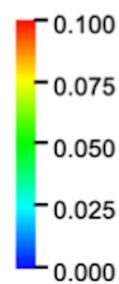
C



OSI (TIWR)	
1	0.00033682
2	0.0020957
3	0.0026673
4	0.00045363
5	0.0018086
6	0.00036471
7	0.0017359
8	0.00047427
9	0.0016562
10	0.00013369
Average	0.00117268

OSI (TKWR)	
1	0.019659
2	0.03551
3	0.016697
4	0.0034354
5	0.0014124
6	0.004953
7	0.0027261
8	0.0047421
9	0.0033357
10	0.0047025
Average	0.00971732

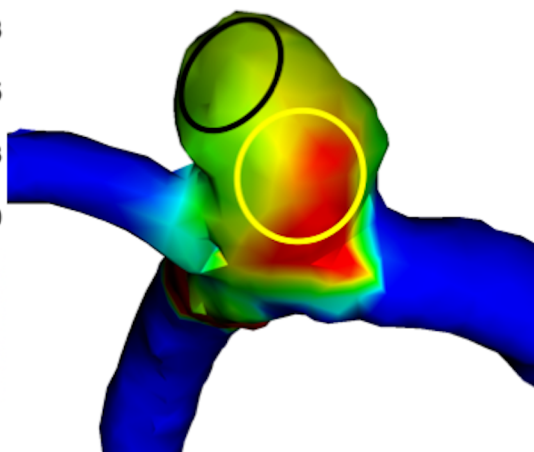
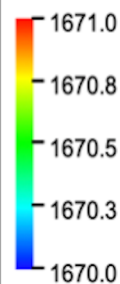
D



TAWSS (TIWR)	
1	0.016858
2	0.017584
3	0.016291
4	0.0086468
5	0.01548
6	0.025144
7	0.020057
8	0.018404
9	0.0123
10	0.017696
Average	0.01684608

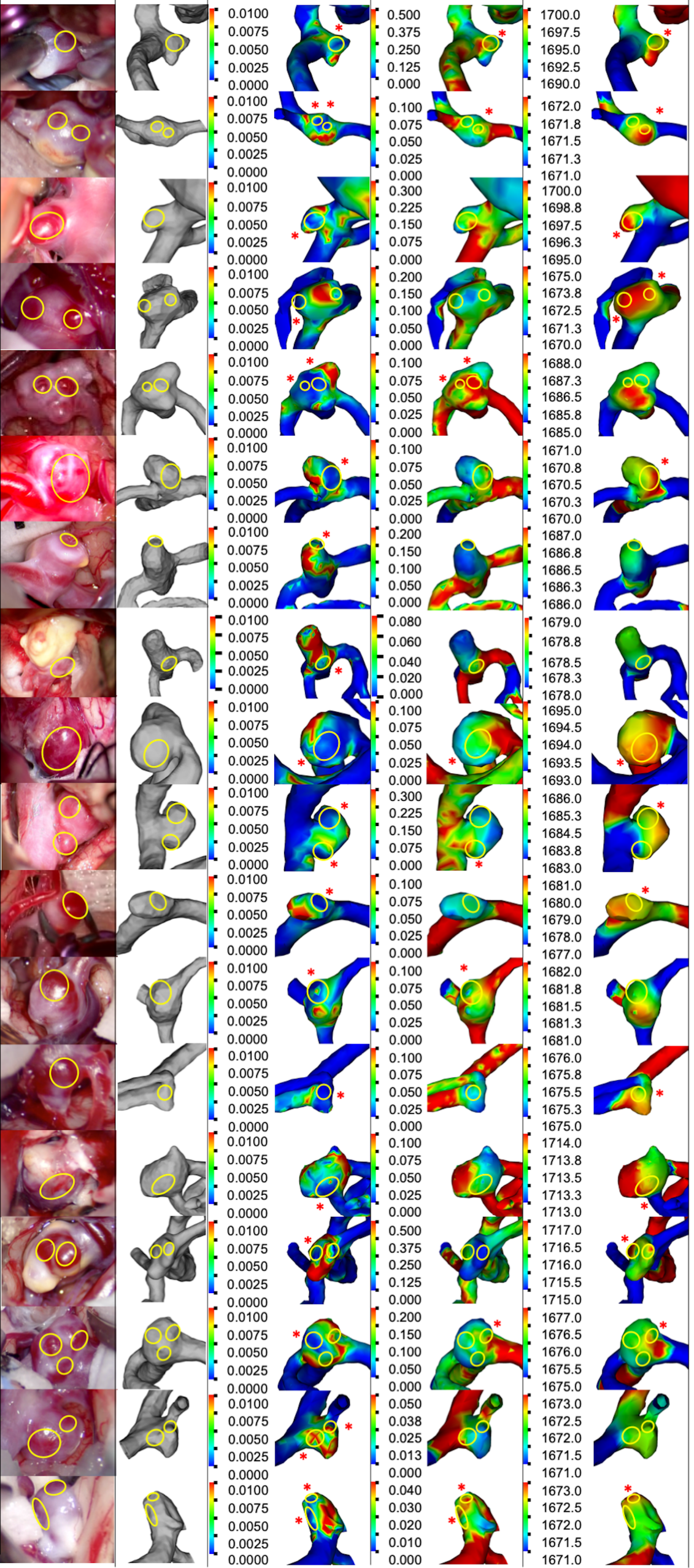
TAWSS (TKWR)	
1	0.060612
2	0.07807
3	0.038561
4	0.028055
5	0.03203
6	0.046524
7	0.05172
8	0.027119
9	0.044527
10	0.063861
Average	0.0471079

E

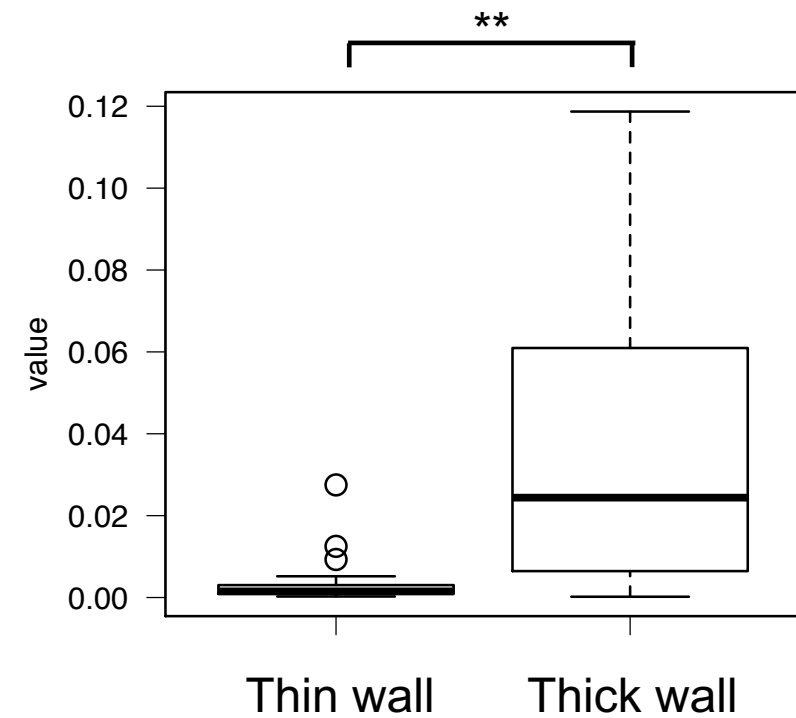


PS (TIWR)	
1	1672
2	1671.65
3	1671.7
4	1671.7
5	1671.9
6	1671.85
7	1672
8	1672.2
9	1671.8
10	1672
Average	1671.88

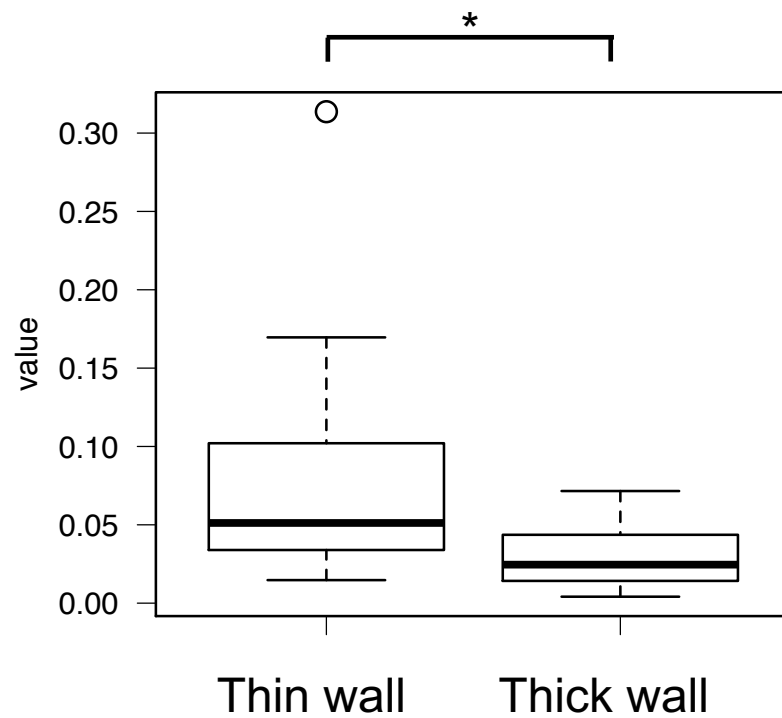
PS (TKWR)	
1	1671.6
2	1671.6
3	1671.65
4	1671.7
5	1671.65
6	1671.65
7	1671.7
8	1671.6
9	1671.6
10	1671.6
Average	1671.635



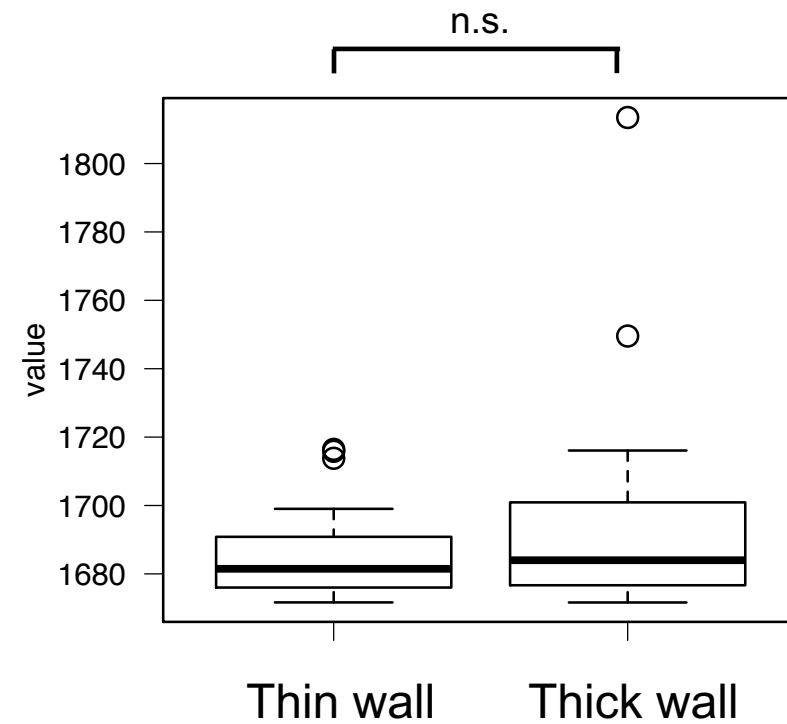
A



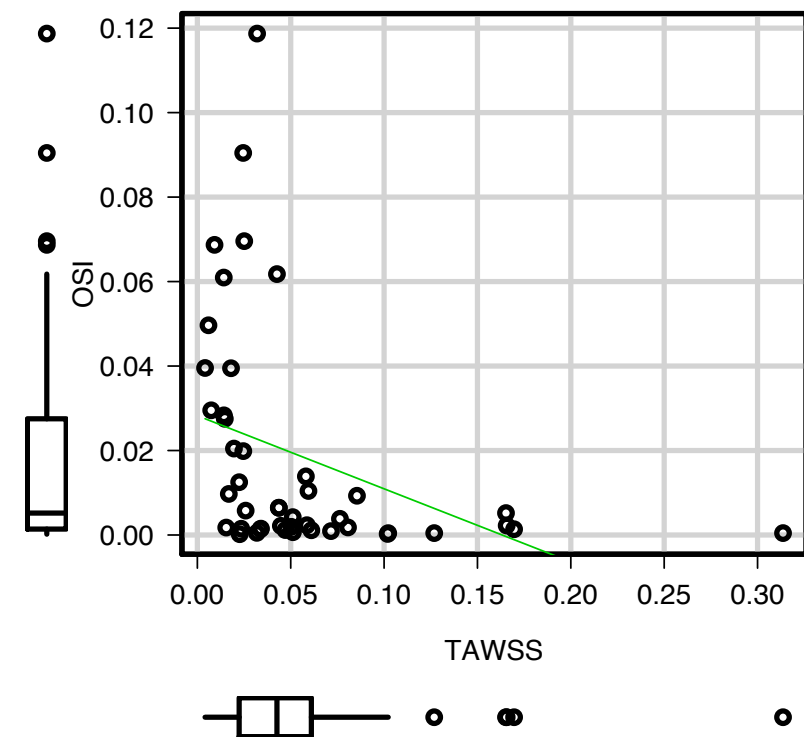
B



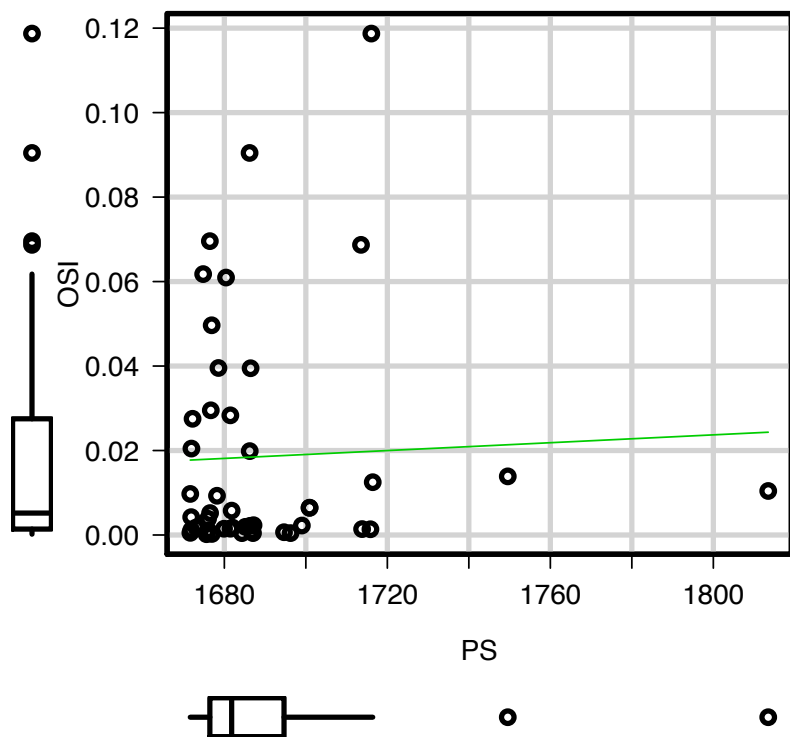
C



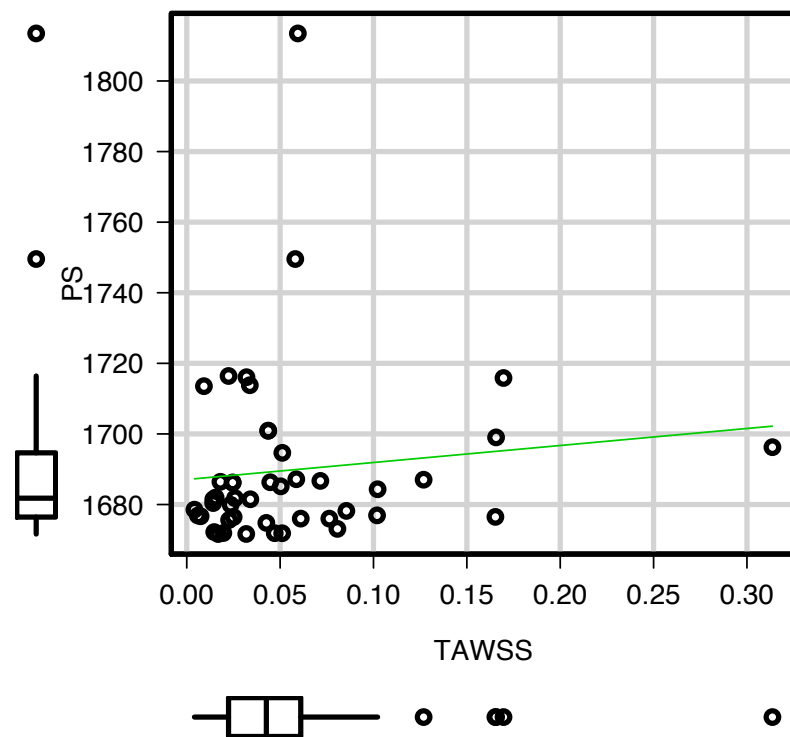
A



B



C



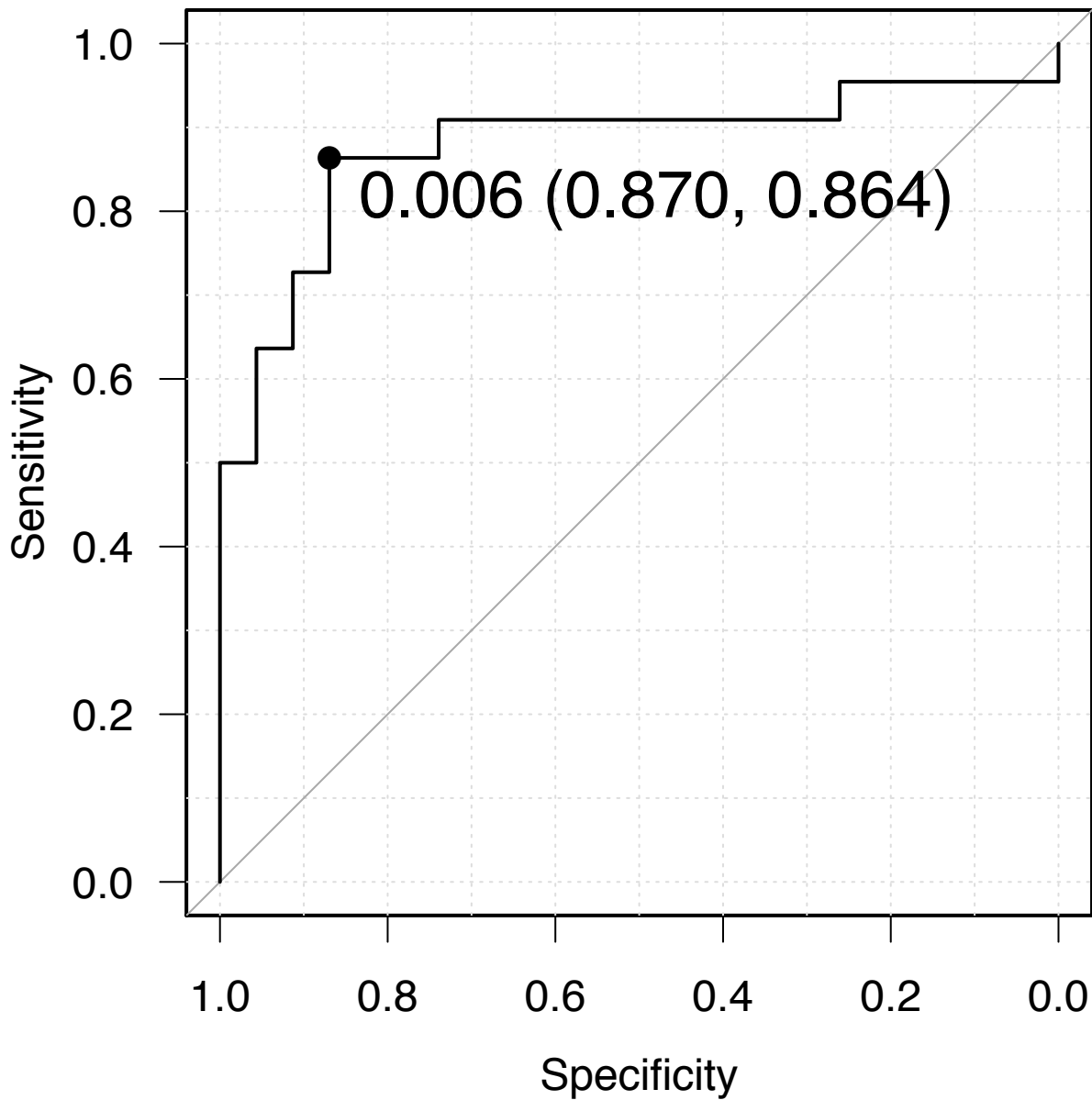


Table1

Baseline characteristics of the patients and aneurysms

Characteristic	No. of cases (%)
Mean patient age (yrs)*	64 ± 12
Sex	
male	7(29.2)
female	17 (70.8)
Right/left	
right	17 (68)
left	8 (32)
Aneurysm location	
MCA	18 (64)
ICA	8 (32)
ACoA	1 (4)
Past history	
Hypertension	10(40)
Dyslipidemia	8 (32)
Current smoking	7 (28)
Diabetes mellitus	4 (16)
Per-oral antiplatelet	2 (8)
Chronic renal failure	2 (8)
Morphological data	
Mean neck diameter (mm)*	3.2 ± 1.2
Mean length (mm)*	5.6 ± 1.7
Mean width (mm)*	4.8 ± 2.1

*Value is presented as the mean ± standard deviation

(ACoA: anterior communicating artery; ICA: internal carotid artery, MCA: middle cerebral artery)

Table 2

ROC curve analysis for oscillatory shear index, time-averaged wall shear stress and pressure					
Parameter	AUC	95% CI	Sensitivity	Specificity	Cut-off Value
OSI	0.875	0.758 - 0.993	0.864	0.87	0.006
TAWSS	0.802	0.675 - 0.93	0.696	0.818	0.045
PS	0.577	0.406 - 0.748	0.318	0.87	1700.915

(AUC: area under the curve; CI, confidence interval; OSI: oscillatory shear index; PS: pressure; ROC: Receiver operating characteristic; TAWSS: time-averaged wall shear stress)

Table 3

Multivariate logistic regression analysis of independent parameters associated with thin-walled regions of the aneurysm dome.

Parameter	Odds ratio	Lower 95%CI	Upper 95%CI	<i>P</i> value
OSI	18.30	3.28	102.00	< 0.001*
TAWSS	0.280	0.0488	1.61	0.154

* Statistically significant

(CI, confidence interval; OSI, oscillatory shear index; TAWSS, time-averaged wall shear stress)